Analysis of Grating-Assisted Directional Couplers Using the Floquet–Bloch Theory

Nai-Hsiang Sun, *Member, IEEE,* Jerome K. Butler, Gary A. Evans, Lily Pang, and Phil Congdon

***Abstract*— The Floquet–Bloch theory is used to develop a theory for grating-assisted directional couplers which predicts the coupled power and coupling lengths and is applicable to lossy waveguides. This theory views grating-assisted directional couplers as conceptually similar to conventional synchronous (nongrating) couplers. In the Floquet–Bloch analysis of the directional coupler, it is necessary to include both proper and improper space harmonics. The determination of which space harmonics are improper is critical to the understanding of the coupler performance. The choice of the improper space harmonics used for the analysis of the coupler is different from that used in contemporary papers.**

I. Introduction

WHEN two identical dielectric waveguides are in close proximity, the composite structure has characteristic modes whose shapes can be approximated from the field shapes of the characteristic modes of the individual waveguides. Accordingly, the modes of the composite structure have power distributions that are predominantly confined to the two "individual" waveguides. Depending upon the nature of excitation of the composite modes, the total power that propagates along the waveguide will be partitioned among the modes. Since the modes propagate at different velocities, the lateral profile of the power distribution will vary along the propagation direction, thus causing a shifting of power from one region to another (or from "one waveguide to another") [1], [2]. The waveguide configuration is known as a directional coupler, and such components are important in many opto-electronic systems [3]. For some applications, such as frequency filters, two nonidentical waveguides with modes which are in synchronism are designed to achieve power transfer over a narrow frequency range [4]. In this case, the two synchronous modes indicate that the two isolated slabs have the same propagation constants of the fundamental mode.

If two nonidentical waveguides in close proximity are not synchronous, a periodic grating structure located between the two waveguides can lead to power transfer between the waveguides. The combination of these two "subwaveguides" and the grating is called a grating-assisted directional coupler (GADC) and can be viewed as a single, composite waveguide. These couplers are important elements for many optical applications such as input–output couplers [5], [6], optical wavelength filters [7]–[10], and wavelength multiplexing devices [11], [12].

Coupled mode theory (CMT) is widely used to analyze grating-assisted directional couplers [13]–[19]. In addition to CMT, a transfer matrix method (TMM) approach uses a mode-matching technique to determine power coupling and scattering in a GADC [20]. However, both the coupled mode theory and the transfer matrix method are based on the assumption that the interacting modes are mutually orthogonal. These approaches give accurate results when the periodic perturbation is weak and the coupled subwaveguides are almost identical (i.e., very similar index profiles and guiding layer thicknesses). On the other hand, the CMT and TMM approach will be less accurate if the grating perturbation is strong, and/or one or more layers of the structure are lossy. Also, the CMT and TMM approaches are inaccurate if one of the modes is leaky.

Recently, investigations of the GADC structure based on a hybrid combination of coupled mode and Floquet–Bloch theory have been discussed [21]–[25]. However, the inclusion of coupled mode theory in these hybrid models limits the applicability and accuracy.

In this paper, we present an accurate approach to the GADC problem based solely on the Floquet–Bloch theory which has been previously used [26]–[30] for the analysis of single mode waveguides with gratings. According to the Floquet–Bloch theory, if a plane wave propagates in an infinite unbounded periodic medium, the complete field pattern should consist of an infinite number of space harmonics. Fig. 1 shows the $\omega - \beta$ diagram for a typical dielectric waveguide without diffraction gratings. The two curves in Fig. 1 indicate the dispersion relations of the zero order mode and the first order mode, labeled as mode A and mode B, respectively. When a grating is a part of the dielectric waveguide, an infinite number of "subdiagrams" are created [31]. Fig. 2 shows two of these $\omega - \beta$ subdiagrams for a periodic dielectric waveguide with a wavevector $K = 2\pi/\Lambda$ where Λ is the grating period. When two space harmonics intersect, strong coupling will occur and lead to energy transfer between modes. Note that at the intersection points the amplitudes of the two harmonics become dominant. Depending on the wavevector K of the grating, two types of coupling, codirectional and contradirectional, can occur. For codirectional coupling, the group velocities of the two coupled harmonics are parallel, whereas the group velocities are antiparallel for contradirectional coupling. Energy is transferred back and forth between two space harmonics which are propagating in the same

Manuscript received March 21, 1997; revised September 9, 1997. This work was supported by DARPA under Contract DAAL01–95–C-3524.

N.-H. Sun, J. K. Butler, and G. A. Evans are with Southern Methodist University, Dallas, TX 75275 USA.

L. Pang and P. Congdon are with Texas Instruments, Dallas, TX 75243 USA.

Publisher Item Identifier S 0733-8724(97)08879-8.

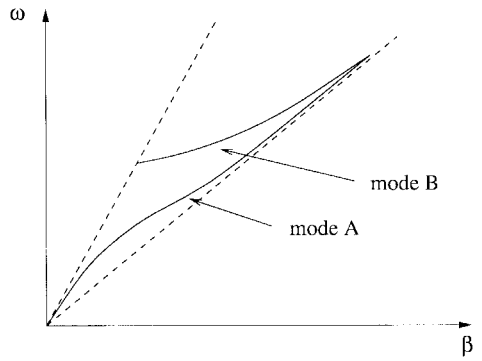

Fig. 1. $\omega - \beta$ plot for a typical dielectric waveguide. "Mode A" indicates the zero order mode, and "mode B" is the first-order mode.

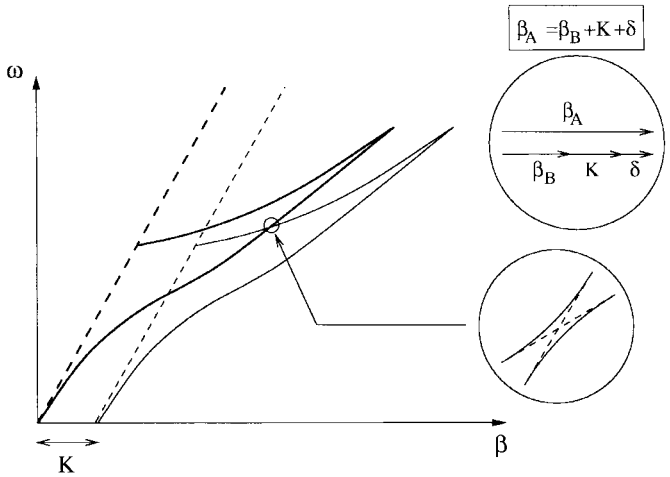

Fig. 2. Codirectional interaction between two space harmonics. The top inset shows the phase matching condition. The bottom inset shows the mode interaction at resonance.

direction (codirectional coupling, illustrated in Fig. 2) or in opposite directions (contradirectional coupling).

By using the Floquet–Bloch theory, the dispersion curves of two coupled modes are calculated in a GADC structure. Fig. 2 illustrates the codirectional coupling of mode A and mode B of a composite GADC waveguide. The resonant condition can be obtained from the dispersion relation (Fig. 2), and the corresponding grating period Λ satisfies

$$\frac{2\pi}{\Lambda} = K = \beta_A = \beta_B - \delta \tag{1}$$

where β_A and β_B are real parts of the propagation constants of the two independent modes. The parameter δ is the *deviation wavenumber* from the nominal resonant condition $K = \beta_A - \beta_B$.

A key point of this paper is that the field distributions of the interacting modes of the GADC waveguide are greatly modified near resonance compared to the field distributions off resonance (which more closely resemble the field distributions of the two modes if the grating was absent from the composite waveguide). In other words, when the grating is present, the partition of power into the two waveguide modes may greatly differ from the power partition in the two modes in the absence of the grating. This superposition of the two field distributions

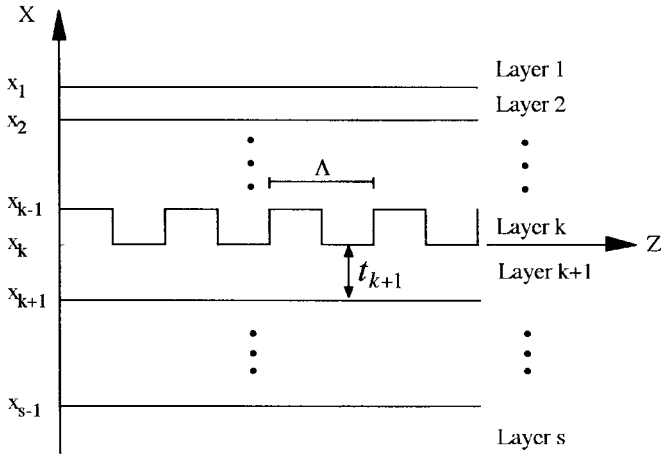

Fig. 3. The basic geometry of the multilayer grating waveguide.

at the input of a directional coupler is the basic concept used to explain synchronous couplers [4] (which do not require a grating to obtain complete power transfer).

The optical distribution at the input of one of the "subwaveguides" may be written as a linear combination of these greatly modified field distributions. From the longitudinal dependence of these two (greatly modified) field distributions, we can obtain the power distribution in the two subwaveguides and hence the distance (the coupling length) over which maximum power is exchanged between the two subwaveguides. If there are no losses, the approximate expression for the coupling length is given by

$$L_c = \frac{\pi}{\delta}. \tag{2}$$

Surprisingly, the coupling length formula (2) is similar to that of conventional (nongrating) synchronous couplers [4].

In Section II a brief derivation of the Floquet–Bloch theory is presented. The branch choices for each space harmonic are discussed in Section III. In Section IV, the analysis of the conventional directional coupler without gratings is reviewed, and in Section V, the field distributions for GADC waveguides near resonance are developed. The coupling length formula is derived in Section VI. In Section VII, we discuss the accuracy of truncating the infinite number of space harmonics.

II. Problem Formulation

The Floquet–Bloch theory used in this study is based on the paper reported by Chang *et al.* [28]. In this section we generalize the Floquet–Bloch approach to composite waveguides with an arbitrary number of layers.

We begin by considering a dielectric waveguide structure with multiple layers and with a grating region as shown in Fig. 3. The superstrate (layer 1) and substrate (layer s) regions are assumed to be half spaces. Layer k is the grating layer with the grating period Λ, x_i is the interface between the ith and $(i+1)$th layer in the x-direction, and t_i is the thickness of the ith layer. For the sake of simplicity it is assumed that the field is invariant with respect to y. The dielectric materials in each layer of Fig. 3 are isotropic and homogeneous. With a time

dependence of the form $\exp(j\omega t)$ being implied, the field in each layer satisfies the scalar Helmholtz equation

$$\left(\frac{\partial^2}{\partial x^2}+\frac{\partial^2}{\partial z^2}\right)F_i(x,z)+\varepsilon_i k_0^2 F_i(x,z)=0 \tag{3}$$

where F_i is the field component ($F_i = E_{yi}$ for TE modes, and $F_i = H_{yi}$ for TM modes), $k_0 = 2\pi/\lambda$ is the free space wavenumber, ε_i is the dielectric constant, and i designates the layer i. The two-dimensional wave function $F_i(x,z)$ is required to appear in the Floquet–Bloch form to satisfy the periodic condition. Since the field is assumed to propagate in the z-direction, the solution of the differential equation (3) becomes

$$\begin{aligned}F_i(x,z)&=\sum_{n=-\infty}^{\infty} f_n^{(i)}(x)\cdot\exp(-jk_{zn}z)\\&=e^{-j(\beta+j\alpha)z}\sum_{n=-\infty}^{\infty} f_n^{(i)}(x)e^{-jnKz}\end{aligned} \tag{4}$$

where

$$k_{zn}=\beta_n+j\alpha=(\beta+nK)+j\alpha. \tag{5}$$

Here $K = 2\pi/\Lambda$ is the grating wavenumber, n is the space harmonic order, and i indicates the ith layer. The value k_{zn} is the complex propagation constant of the nth spatial harmonic. The real part of k_{zn}, β_n, is the phase constant of the nth space harmonic, and the imaginary part of k_{zn}, α ($\alpha<0$), is the attenuation constant due to the leakage of the guided-wave energy into the substrate and the superstrate regions.

A. Field Solutions Outside the Grating Region

In the uniform layers above and below the grating, we can use the transfer matrix method to solve (3). The 2-D Helmholtz equation can be converted into the 1-D differential equation

$$\frac{d^2 f_n^{(i)}(x)}{dx^2}+[\varepsilon_i k_0^2-k_{zn}^2]f_n^{(i)}(x)=0. \tag{6}$$

The complex transverse wavenumber is written as $k_{xn}^{(i)}$ and is defined by

$$(k_{xn}^{(i)})^2=\varepsilon_i k_0^2-k_{zn}^2 \tag{7}$$

or

$$k_{xn}^{(i)}=\pm\sqrt{\varepsilon_i k_0^2-k_{zn}^2} \tag{8}$$

so (6) becomes

$$\frac{d^2 f_n^{(i)}(x)}{dx^2}+(k_{xn}^{(i)})^2 f_n^{(i)}(x)=0. \tag{9}$$

The solutions of (9) are given by

$$f_n^{(i)}(x)=\begin{cases}b_n^{(1)}\exp[-jk_{xn}^{(1)}x] & i=1\\ a^{(i)}\exp[jk_{xn}^{(i)}x]+b_n^{(i)}\exp[-jk_{xn}^{(i)}(x)] & \\ \qquad\qquad i=2\sim s-1, \quad i\neq k & \\ a_n^{(s)}\exp[jk_{xn}^{(s)}x] & i=s\end{cases} \tag{10}$$

where $a_s^{(i)}$ and $b_n^{(i)}$ are amplitude coefficients. Note that the transverse wave is considered to propagate away from the structure in the semi-infinite layers. Hence, $a_n^{(1)}$is zero in the superstrate layer and $b_n^{(s)}$ is zero in the substrate layer. The signs of the transverse wavenumbers in the superstrate and substrate layer, $k_{xn}^{(1)}$ and $k_{xn}^{(s)}$, must be carefully chosen in order to obtain physically meaningful solutions as discussed in Section III.

In solving the electromagnetic problem, the boundary condition should be applied to each interface of the structure. Consider only the boundary condition outside the grating layer. The field components $f_n^{(i)}(x)$ and $f_n^{(i+1)}(x)$ must be continuous at the boundary $x = x_i$ where $i = 1 \sim s-1$ but $i \neq k$ and $i \neq k-1$. In addition, the normal derivative field components: $df_n^{(i)}(x)/dx$ and $df_n^{(i+1)}(x)/dx$ for TE modes, and $(1/\varepsilon_i)\,df_n^{(i)}(x)/dx$ and $(1/\varepsilon_{i+1})\,df_n^{(i+1)}(x)/dx$ for TM modes, must also be continuous at the boundaries. We define $\overline{C}_n^{(i)}$ and $\overline{C}_n^{(n+1)}$ to be the amplitude coefficient vectors of layer (i) and layer $(i+1)$ with the nth space harmonic. They are expressed as

$$\overline{C}_n^{(i)}=\begin{pmatrix}a_n^{(i)}\\ b_n^{(i)}\end{pmatrix} \quad \text{and} \quad \overline{C}_n^{(i+1)}=\begin{pmatrix}a_n^{(i+1)}\\ b_n^{(i+1)}\end{pmatrix}.$$

At the boundary $x = x_i$, the relationship between $\overline{C}_n^{(i)}$ and $\overline{C}_n^{(i+1)}$ is

$$\boldsymbol{T}_n^{(i)}\overline{C}_n^{(i)}=\boldsymbol{M}_n^{(i+1)}\overline{C}_n^{(i+1)} \tag{11}$$

where $\boldsymbol{T}_n^{(i)}$ and $\boldsymbol{M}_n^{(i+1)}$ are 2×2 transfer matrices shown at the bottom of the page.

According to (11), coefficients in layer (i) can be substituted by those in either layer $(i-1)$ or layer $(i+1)$. Consider

$$\boldsymbol{T}_n^{(i)}=\begin{cases}\begin{bmatrix}\exp(jk_{xn}^{(i)}x_i) & \exp(-jk_{xn}^{(i)}x_i)\\ jk_{xn}^{(i)}\exp(jk_{xn}^{(i)}x_i) & -jk_{xn}^{(i)}\exp(jk_{xn}^{(i)}x_i)\end{bmatrix} & \text{(For TE)}\\ \begin{bmatrix}\exp(jk_{xn}^{(i)}x_i) & \exp(-jk_{xn}^{(i)}x_i)\\ \dfrac{jk_{xn}^{(i)}}{\varepsilon_i}\exp(jk_{xn}^{(i)}x_i) & -\dfrac{jk_{xn}^{(i)}}{\varepsilon_i}\exp(jk_{xn}^{(i)}x_i)\end{bmatrix} & \text{(For TM)}\end{cases}$$

$$\boldsymbol{M}_n^{(i+1)}=\begin{cases}\begin{bmatrix}\exp(jk_{xn}^{(i+1)}x_i) & \exp(-jk_{xn}^{(i+1)}x_i)\\ jk_{xn}^{(i+1)}\exp(jk_{xn}^{(i+1)}-x_i) & -jk_{xn}^{(i+1)}\exp(jk_{xn}^{(i+1)}x_i)\end{bmatrix} & \text{(For TE)}\\ \begin{bmatrix}\exp(jk_{xn}^{(i+1)}x_i) & \exp(-jk_{xn}^{(i+1)}x_i)\\ \dfrac{jk_{xn}^{(i+1)}}{\varepsilon_{i+1}}\exp(jk_{xn}^{(i+1)}x_i) & -\dfrac{jk_{xn}^{(i+1)}}{\varepsilon_{i+1}}\exp(jk_{xn}^{(i+1)}x_i)\end{bmatrix} & \text{(For TM)}\end{cases}$$

the boundary above the grating layer. The coefficient of layer $(k-1)$ with the nth space harmonic becomes

$$\begin{aligned}\overline{C}_n^{(k-1)} &= (\boldsymbol{M}_n^{(k-1)})^{-1}\boldsymbol{T}_n^{(k-2)}\overline{C}_n^{(k-2)} \\ &= \boldsymbol{S}_n^{(k-2)}\overline{C}_n^{(k-2)} \\ &= \boldsymbol{S}_n^{(k-2)}\cdot\boldsymbol{S}_n^{(1)}\overline{C}_n^{(1)} \\ \overline{C}_n^{(k-1)} &= \boldsymbol{S}_n\overline{C}_n^{(1)} \end{aligned} \tag{12}$$

where $\boldsymbol{S}_n^{(k-2)} = (\boldsymbol{M}_n^{(k-1)})^{-1}\boldsymbol{T}_n^{(k-2)}$. $\boldsymbol{S}_n$ is the two by two transfer matrix between $\overline{C}_n^{(k-1)}$ and $\overline{C}_n^{(1)}$. Because $a_n^{(1)}$ is zero, $\overline{C}_n^{(k-1)}$ can be expressed as

$$\overline{C}_n^{(k-1)} = \begin{pmatrix} a_n^{(k-1)} \\ b_n^{(k-1)} \end{pmatrix} = \begin{pmatrix} s_{n12}b_n^{(1)} \\ s_{n22}b_n^{(1)} \end{pmatrix} \tag{13}$$

where s_{n12} and s_{n22} are the matrix elements of $\boldsymbol{S}_n$. A similar relationship between $\overline{C}_n^{(k+1)}$ and $a_n^{(s)}$ can be found by the same procedure. For the boundary below the grating layer, the coefficient of layer $(k+1)$ with the nth space harmonic becomes

$$\begin{aligned}\overline{C}_n^{(k+1)} &= (\boldsymbol{T}_n^{(k+1)})^{-1}\boldsymbol{M}_n^{(k+2)}\overline{C}_n^{(k+2)} \\ &= \boldsymbol{R}_n^{(k+2)}\cdots\boldsymbol{R}_n^{(s)}\overline{C}_n^{(s)} \\ \overline{C}_n^{(k+1)} &= \boldsymbol{R}_n\overline{C}_n^{(s)} \end{aligned} \tag{14}$$

where $\boldsymbol{R}_n^{(k+2)} = (\boldsymbol{T}_n^{(k+1)})^{-1}\boldsymbol{M}_n^{(k+2)}$. From (10), $b_n^{(s)}$ is zero, so elements of $\overline{C}_n^{(k+1)}$ can be replaced by $a_n^{(s)}$:

$$\overline{C}_n^{(k+1)} = \begin{pmatrix} a_n^{(k+1)} \\ b_n^{(k+1)} \end{pmatrix} = \begin{pmatrix} r_{n11}a_n^{(s)} \\ r_{n21}a_n^{(s)} \end{pmatrix}. \tag{15}$$

B. Field Solutions Inside the Grating Region

Although the grating can be (and usually is) a periodic boundary between two distinct layers, we always consider the region defined by the height of the grating to be a separate layer (or region) of the composite waveguide. Inside the grating region, the solution provides most of the interesting features of the present problem because dielectric constants are nonuniform and vary periodically. Although the corresponding field of the grating region still satisfies the Helmholtz equation, we now have to account for a periodic permittivity which can be written in terms of the Fourier series as

$$\varepsilon(x,z) = \sum_n \varepsilon_n(x)\cdot\exp(j2\pi nz/\Lambda) \tag{16a}$$

$$\varepsilon(x,z)^{-1} = \sum_n \xi_n(x)\cdot\exp(j2\pi nz/\Lambda). \tag{16b}$$

For the grating structure, the problem is addressed by solving the equivalent Maxwell's equations instead of the Helmholtz equation

$$\frac{dF}{dx} = QG \tag{17a}$$

$$\frac{dG}{dx} = PF \tag{17b}$$

where $F = E_y$ for TE, $F = H_y$ for TM, and $G = H_z$ for TE, $G = E_z$ for TM. F and G are expressed as

$$F = F_k(x,z) = \sum_{n=-\infty}^{\infty} f_n^{(k)}(x)\cdot\exp(-jk_{zn}z) \tag{18a}$$

$$G = G_k(x,z) = \sum_{n=-\infty}^{\infty} g_n^{(k)}\cdot(x)\cdot\exp(-jk_{zn}z). \tag{18b}$$

Note that the fields $f_n^{(k)}(x)$ and $g_n^{(k)}(x)$ in (18) are coupled together with their spatial harmonics. Therefore, when we substitute (18) into (17), the fields inside the grating region become

$$\frac{d\overline{f}(x)}{dx} = \boldsymbol{Q}(k_{z0})\overline{g}(x) \tag{19a}$$

$$\frac{d\overline{g}(x)}{dx} = \boldsymbol{P}(k_{z0})\overline{f}(x) \tag{19b}$$

where k_{z0} is the propagation constant of the zeroth spatial harmonics. The vectors $\overline{f}(x)$ and $\overline{g}(x)$ are formed by the field of spatial harmonics $f_n^{(k)}(x)$ and $g_n^{(k)}(x)$, respectively, and are written

$$\overline{f}(x) = \begin{pmatrix} f_{-j_1}^{(k)}(x) \\ \vdots \\ f_0^{(k)}(x) \\ \vdots \\ f_{j_2}^{(k)}(x) \end{pmatrix} \tag{20a}$$

$$\overline{g}(x) = \begin{pmatrix} g_{-j_1}^{(k)}(x) \\ \vdots \\ g_0^{(k)}(x) \\ \vdots \\ g_{j_2}^{(k)}(x) \end{pmatrix}. \tag{20b}$$

Note that the vectors $\overline{f}(x)$ and $\overline{g}(x)$ consist of $l = j_1 + j_2 + 1$ space harmonic components, and $\boldsymbol{P}(k_{z0})$ and $\boldsymbol{Q}(k_{z0})$ are $l \times l$ matrices with elements

$$p_{nm} = \begin{cases} j\omega\varepsilon_0\left[\left(\frac{k_{zn}}{k_0}\right)^2\delta_{nm} - \varepsilon_{n-m}\right] & \text{(for TE)} \\ j\omega\mu_0\left[\delta_{nm} - \left(\frac{k_{zn}k_{zm}}{k_0^2}\right)\xi_{n-m}\right] & \text{(for TM)} \end{cases} \tag{21}$$

$$q_{nm} = \begin{cases} -j\omega\mu_0\delta_{nm} & \text{(for TE)} \\ j\omega\varepsilon_0\varepsilon_{n-m} & \text{(for TM)} \end{cases} \tag{22}$$

where k_{zn} is the propagation constant for the nth space harmonic, ε_{n-m} and ξ_{n-m} is the $(n-m)$th term in (16), and δ_{nm} is the Kronecker's delta function ($\delta_{nm} = 1$ when $n = m$, and $\delta_{nm} = 0$ when $n \neq m$). Equation (19) consists of two systems of first-order linear constant coefficient ordinary differential equations. We can reduce (19) into one system of first-order linear ordinary differential equations as follows:

$$\frac{d}{dx}\begin{pmatrix}\overline{f}(x) \\ \overline{g}(x)\end{pmatrix} = \boldsymbol{A}(k_{z0})\begin{pmatrix}\overline{f}(x) \\ \overline{g}(x)\end{pmatrix}. \tag{23}$$

where

$$\boldsymbol{A}(k_{z0}) = \begin{pmatrix} 0 & \boldsymbol{Q}(k_{z0} \\ \boldsymbol{P}(k_{z0}) & 0 \end{pmatrix} \tag{24}$$

is a square matrix. In this paper, (23) is solved by the fourth-order Runge–Kutta method (RKM) [32], instead of the Adams–Moulton method (AMM) used in [28], because the RKM is faster and more stable than the AMM. The numerical solution of (23) gives the field values within the grating region in terms of the field values at the grating boundary. Since $\overline{f}(x_{k-1})$ is the initial value of the field in the grating layer, $\overline{f}(x)$ and $\overline{g}(x)$ at $x = x_k$ can be written as

$$\overline{f}(x_k) = \boldsymbol{Y}_f(k_{z0})\overline{f}(x_{k-1}) \tag{25a}$$

$$\overline{g}(x_k) = \boldsymbol{Y}_g(k_{z0})\overline{f}(x_{k-1}) \tag{25b}$$

where $\boldsymbol{Y}_f(k_{z0})$ and $\boldsymbol{Y}_g(k_{z0})$ are l × l matrices given by the Runge–Kutta method (see Appendix).

C. The Characteristic Equation

The characteristic equation (which will provide the dispersion relation) of the GADC structure is obtained by matching the boundary conditions at both grating layer interfaces.

First, we obtain the field distributions in the layers immediately adjacent to the grating layers, layer $(k-1)$ and layer $(k+1)$. Inserting (13) into (10) relates the field distribution of the nth spatial harmonic in the layer $(k-1)$ to the field amplitudes $b_n^{(1)}$ in the superstrate

$$f_n^{(k-1)}(x) = [s_{n12}\exp(jk_{xn}^{(k-1)}x) + s_{n22}\exp(-jk_{xn}^{(k-1)}x)]b_n^{(1)}. \tag{26}$$

Similarly, by substituting (15) into (10), the field distribution of the nth spatial harmonic in layer $(k+1)$ is related to the field amplitudes $a_n^{(s)}$ in the substrate

$$f_n^{(k+1)}(x) = [r_{n11}\exp(jk_{xn}^{(k+1)}x) + r_{n12}\exp(-jk_{xn}^{(k+1)}x)]a_n^{(s)}. \tag{27}$$

Matching (18)–(26) at $x = x_{k-1}$ results (after some calculation) in the boundary condition

$$\boldsymbol{U}(x_{k-1})\cdot\frac{d\overline{f}(x_{k-1})}{dx} = \boldsymbol{V}(x_{k-1})\cdot\overline{f}(x_{k-1}) \tag{28}$$

where $\boldsymbol{U}(x_{k-1})$ and $\boldsymbol{V}(x_{k-1})$ are square matrices, and their sizes depend on the number of spatial harmonics. The elements of matrices $\boldsymbol{U}(x_{k-1})$ and $\boldsymbol{V}(x_{k-1})$ are expressed as

$$u_{n-j_1+1,m-j_1+1} = \begin{cases}\delta_{nm} & \text{(for TE)}\\ \xi_{n-m} & \text{(for TM)}\end{cases} \tag{29}$$

$$v_{n-j_1+1,m-j_1+1} = \frac{t_{n21}^{(k-1)}s_{n12} + t_{n22}^{(k-1)}s_{n22}}{t_{n11}^{(k-1)}s_{n12} + t_{n12}^{(k-1)}s_{n22}}\delta_{nm} \tag{30}$$

where n and m indicate the nth and mth space harmonics of the series, and the spatial harmonics are truncated from $-j_1$ to j_2 ($n = -j_1,\cdots,j_2$ and $m = -j_1,\cdots,j_2$). Note that $v_{n-j_1+1,m-j_1+1}$ is valid for both TE and TM modes. $t_{n11}^{(k-1)}, t_{n12}^{(k-1)}, t_{n21}^{(k-1)}$, and $t_{n22}^{(k-1)}$ are elements of matrix $\boldsymbol{T}_n^{(k-1)}$ [see (11)].

Similarly, matching (18)–(27) at $x = x_k$ results in the boundary condition

$$\boldsymbol{U}(x_k)\cdot\frac{d\overline{f}(x_k)}{dx} = \boldsymbol{W}(x_k)\cdot\overline{f}(x_k). \tag{31}$$

The elements of matrices $\boldsymbol{U}(x_k)$ has the same expressions as (29), and the elements of $\boldsymbol{W}(x_k)$ are

$$w_{n-j_1+1,m-j_1+1} = \frac{m_{n21}^{(k)}r_{n11} + m_{n22}^{(k)}r_{n21}}{m_{n11}^{(k)}r_{n11} + m_{n12}^{(k)}r_{n21}}\delta_{nm} \tag{32}$$

where $m_{n11}^{(k)}, m_{n12}^{(k)}, m_{n21}^{(k)}$, and $m_{n22}^{(k)}$ are elements of matrix $\boldsymbol{M}_n^{(k)}$ [see (11)]. Combining (25), (28), and (31), we obtain the characteristic equation [28]

$$\boldsymbol{D}(k_{z0})\cdot\overline{f}(x_{k-1}) = 0 \tag{33}$$

where $\boldsymbol{D}(k_{z0}) = [\boldsymbol{U}(x_k)\cdot\boldsymbol{Q}(k_{z0})\cdot\boldsymbol{Y}_g(k_{z0}) - \boldsymbol{W}(x_k)\cdot\boldsymbol{Y}_f(k_{z0})]$ is a $l \times l$ matrix, $\overline{f}(x_{k-1})$ is the initial value of the field in the grating layer, and the unknown variable k_{z0} is the complex propagation constant. The system of linear equations will have a nontrivial solution when the determinant of matrix $\boldsymbol{D}(k_{z0})$ is equal to zero. The solutions of the determinant equation

$$\det[\boldsymbol{D}(k_{z0})] = 0 \tag{34}$$

will give the propagation constants for the modes of the structure. The complex roots k_{z0} can be found by Muller's method. The Floquet amplitudes for the field distribution in all the uniform regions can subsequently be evaluated from (33).

III. Branch Choices for Transverse Wavevectors

Choosing the correct signs in (8) is critical in obtaining the correct complex roots of the determinant (34), since the sign choice determines whether the field distribution of the nth spatial harmonic will be proper or improper. We introduce a modified rule for general periodic waveguides to supplement the conventional rule [31], [33] that applies to choosing branch cuts in lossless periodic waveguides.

The conventional rule requires that the loci of k_{zn} in the complex plane must be traced continuously to produce smooth curves as a function of a defined physical parameter. Assuming that lossless materials are in the semi-infinite regions of the superstrate $(x > x_1)$ and substrate $(x < x_{s-1})$, we only need to determine the signs of the two transverse space harmonic propagation constants, $k_{xn}^{(1)}$ and $k_{xn}^{(s)}$, in the superstrate and substrate. Since $k_{xn}^{(1)}$ and $k_{xn}^{(s)}$ are double-valued functions of k_{zn}, different solutions exist corresponding to the choice of sign in (8). For the superstrate, the choice for $k_{xn}^{(1)}$ has previously been prescribed by requiring that all the positive spatial harmonics $(n \geq 0)$ in the field represent proper waves, i.e.

$$\text{Im}(k_{xn}^{(1)}) < 0 \quad \text{for} \quad n \geq 0. \tag{35}$$

In cases where the space harmonics are negative $(n < 0)$, $k_{xn}^{(1)}$ corresponded to proper waves if β_n is negative

$$\text{Im}(k_{xn}^{(1)}) < 0 \quad \text{if Re}[\beta_n] \leq 0 \quad \text{for} \quad n < 0 \tag{36a}$$

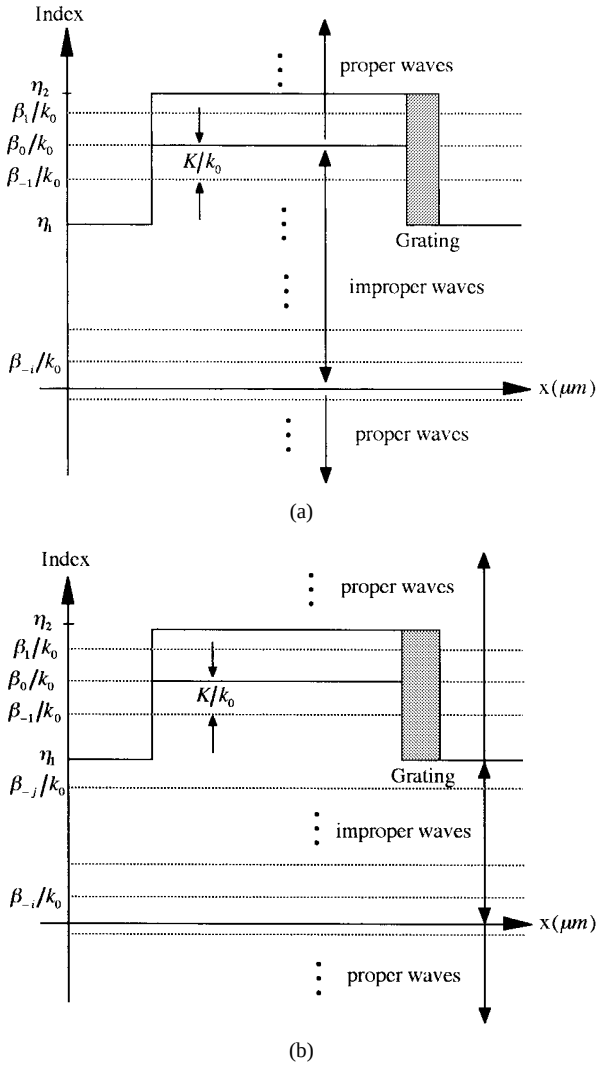

Fig. 4. (a) The index profile of a symmetric four-layer dielectric waveguide. The grating layer is shaded. According to the conventional rule, the $n=-1$ to $-i$ harmonics are improper waves. (b) The index profile of a symmetric four-layer dielectric waveguide. The grating layer is shaded. According to our modification of the conventional rule, the $n=-j$ to $-i$ harmonics are improper waves.

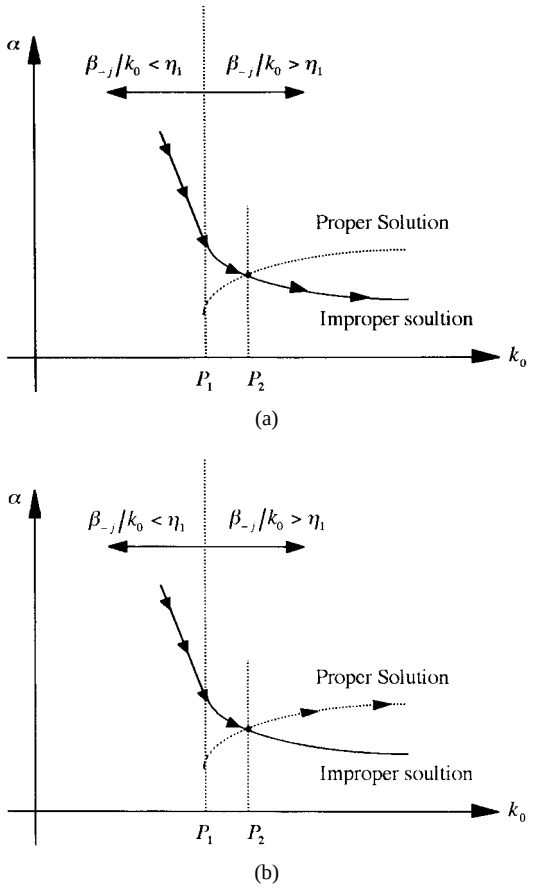

Fig. 5. (a) The arrows on the solid lines indicate the locus of α chosen by the conventional rule (36) as a function of wavenumber k_0. (b) The arrows on the solid lines ($k_0 < P_2$) and dotted lines ($k_0 > P_2$) indicate the locus of α chosen by the modified rule as a function of wavenumber k_0.

and to improper waves if β_n is positive [34]

$$\text{Im}\,(k_{xn}^{(1)}) > 0 \quad \text{if Re}\,[\beta_n] > 0 \quad \text{for} \quad n < 0. \tag{36a}$$

This rule is also applied to the choice of the branch cuts in the substrate region.

In lossless materials around the second Bragg, the above rule presents accurate results [26], [28]–[29], [34]. However, when λ/Λ is much less than one, we show that this rule needs to be modified, by considering a simple four-layer lossless dielectric waveguide which includes a grating layer. The index profile is shown in Fig. 4 where the uniform layers have refractive indexes of η_1, η_2, and η_1. We define the smallest positive effective index to be the ith harmonic (i.e., $(\beta_{-i-1}/k_0) < 0$ and $(\beta_{-i}/k_0) > 0$), and the effective index of the $-j$th harmonic to be just less than η_1 (i.e., $(\beta_{-j+1}/k_0) > \eta_1 > (\beta_{-j}/k_0)$). Fig. 4(a) shows that, according to the conventional rule, the harmonics of $n=-1$ to $-i$ correspond to improper waves. However, as shown in Fig. 4(b), the $n=-1$ to $(-j+1)$ harmonics should represent proper waves because their effective indices are above the index of the substrate η_1. This observation suggests that the proper or improper property of each space harmonic should not be related to the sign of the space harmonic n but should correspond to the location of the effective index. If the effective index of a space harmonic is greater than η_1, it represents a proper mode even though n is negative. Thus, our modification to the conventional rule states that the $n=-1$ to $(-j+1)$ harmonics should be chosen as proper waves.

The value of the propagation constant should vary continuously with the free space wavenumber k_0. Fig. 5(a) shows an example of the attenuation constant α as a function of k_0. Assume that the effective index of the $-j$ space harmonic is equal to η_1 ($\beta_{-j}/k_o = \eta_1$) when k_0 is equal to P_1. The locus of α chosen by the conventional rule (36) is shown in Fig. 5(a). In this case the $n=-j$ harmonic represents the improper wave whether k_0 is greater than or less than P_1. However, as shown in Fig. 5(a), according to the modified rule, the $-j$ space harmonic should change from an improper wave to a proper wave at $k_0 = P_1$ as k_0 varies from to $k_0 < P_1$ to $k_0 > P_1$.

Unfortunately, from Fig. 5(a), a discontinuity of the locus of the attenuation occurs at $k_0 = P_1$. Although our first modification to the conventional rule correctly chooses the

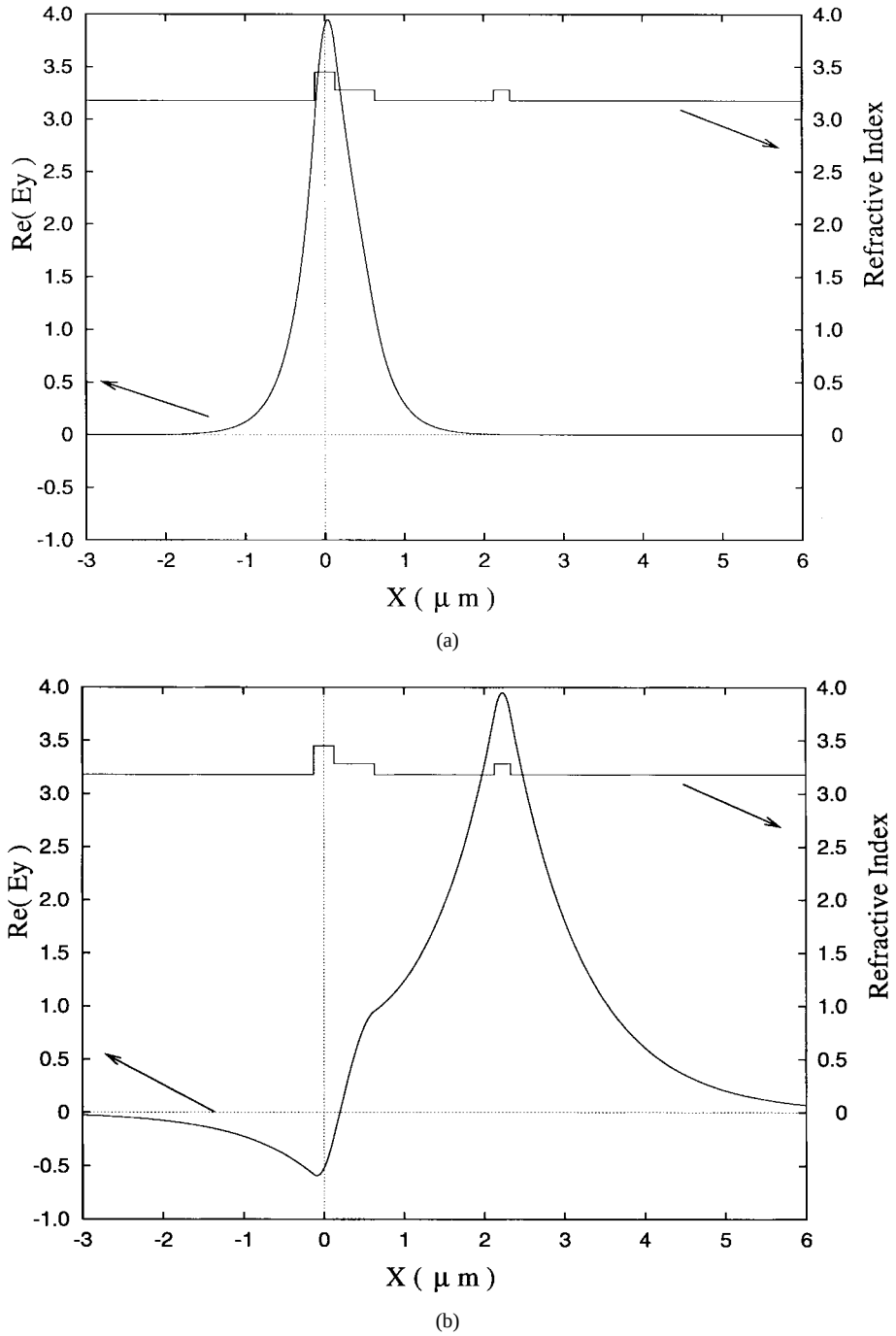

Fig. 6. The components of (a) mode A and (b) mode B for TE modes. The index profile is also shown. The parameters are listed in Table I.

branches, we now have a discontinuity of the propagation constant k_{zn} at P_1. To resolve the discontinuity problem, we notice that both the improper and proper $n = -j$ space harmonics have almost identical values of β_{-j} when k_0 is greater than P_1. More importantly, the point $k_0 = P_2$ corresponds to a double root of the propagation constant. Hence, we further modify the conventional rule to require a branch change of the $-j$th harmonic at $k_0 = P_2$. This choice for the branch change is consistent with having the loci of the propagation constant continuous as k_0 is varied, as shown in Fig. 5(b). In practice, the region $P_1 < k_0 < P_2$ is very narrow and can often be ignored.

IV. Nongrating Directional Couplers

The conventional (nongrating) directional coupler used in integrated optics consists of two synchronous subwaveguides. There are always two lowest order solutions of the composite waveguide with propagation constants β_A and β_B. For TE polarization, the E_y components of the two modes have even and odd symmetry. Thus, the two modes can be added so that their fields nearly cancel in one subwaveguide at the input end of the coupler. However, in the other subwaveguide, the two fields reinforce each other, representing light confined one subwaveguide. Since the zero order mode and the first

TABLE I
PARAMETERS FOR A DIRECTIONAL COUPLER WITH TWO NONIDENTICAL SUBWAVEGUIDES [14]

	Thickness (μm)	Refractive Index
Layer 1 (Superstrate)	∞	3.180
Layer 2 (Sub-waveguide B)	$t_2 = 0.200$	3.282
Layer 3	$t_3 = 1.500$	3.180
Layer 4	$t_4 = 0.500$	3.282
Layer 5 (Sub-waveguide A)	$t_5 = 0.257$	3.450
Layer 6 (Substrate)	∞	3.180

order mode have slightly different propagation constants, their relative phases will reverse at a distance $L_c = \pi/(\beta_A - \beta_B)$. At this point, the two fields reinforce each other in the opposite subwaveguide and the light has been totally coupled to the other subwaveguide.

Assume now that the (nongrating) directional coupler is made of two nonidentical subwaveguides with propagation constants of the fundamental mode for each subwaveguide given by β_a and β_b. Complete power exchange between the two subwaveguides occurs when the fundamental modes of the two separate subwaveguides have the same propagation constants $(\beta_a = \beta_b)$. If the modes of the composite structure of this directional coupler are calculated, the two lowest order modes of the directional coupler have slightly different propagation constants $(\beta_A \approx \beta_B)$ with the coupling length of $L_c = \pi/(\beta_A - \beta_B)$ [4].

If the fundamental modes of the two isolated subwaveguides have significantly different propagation constants $(\beta_a \neq \beta_b)$, very little power will be exchanged between the two subwaveguides. Table I shows a structure consisting of two nonidentical subwaveguides (without a grating), which is discussed by Marcuse [14]. The composite structure of this directional coupler has different propagation constants $(\beta_A \neq \beta_B)$. The E_y components of the two lowest order modes (modes A and B) for the TE modes are shown in Fig. 6. Note that the field patterns of modes A and B are confined mainly to either subwaveguide A or subwaveguide B. Although the input distribution of one subwaveguide can be approximated as a linear superposition of the field distribution of the two lowest order composite modes, only one mode receives a significant portion of the input power. (This is in contrast to synchronous couplers where each composite mode has nearly equal power distribution in each subwaveguide.) In short, an effective directional coupler can be made only if the input power is distributed nearly equally among the two modes.

V. GRATING-ASSISTED DIRECTIONAL COUPLERS

Significant power exchange can occur between two nonsynchronous subwaveguides which have different propagation constants if a diffraction grating is incorporated in the intermediate region between the two waveguides. This structure, called a grating-assisted directional coupler (GADC) and shown in Fig. 7, is made of two nonidentical waveguides, referred to as "subwaveguide A" and "subwaveguide B," and a grating layer. By using the Floquet–Bloch theory discussed

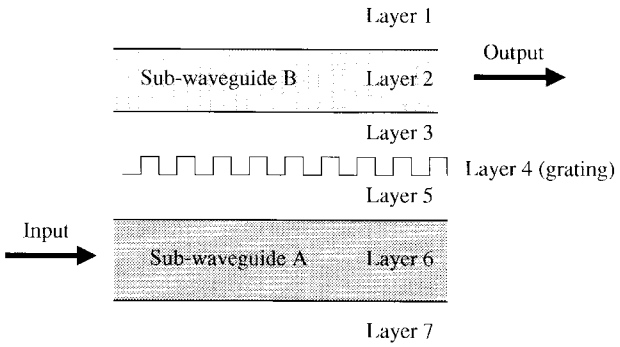

Fig. 7. Sketch of a grating-assisted directional coupler.

TABLE II
PARAMETERS FOR A GRATING-ASSISTED DIRECTIONAL COUPLER WITH TWO NONIDENTICAL SUBWAVEGUIDES [14]

	Thickness (μm)	Refractive Index
Layer 1 (Superstrate)	∞	3.180
Layer 2 (Sub-waveguide B)	$t_2 = 0.200$	3.282
Layer 3	$t_3 = 1.450$	3.180
Layer 4 (Grating)	$t_4 = 0.100$	3.180 / 3.282
Layer 5	$t_5 = 0.450$	3.282
Layer 6 (Sub-waveguide A)	$t_6 = 0.257$	3.450
Layer 7 (Substrate)	∞	3.180

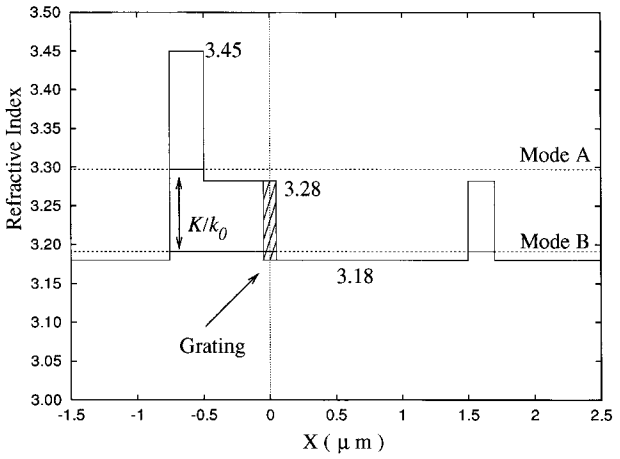

Fig. 8. The index profile of the grating-assisted directional coupler described in Table II and shown in Fig. 7. The two dashed lines correspond to the effective index of mode A ($\approx$3.30) and mode B ($\approx$3.19).

in Section II, rigorous solutions of the propagation constants and the complete field distributions for the GADC structure are found.

Consider the GADC structure analyzed by Marcuse [14]. The refractive index and the thickness of each layer are shown in Table II and Fig. 8. The vacuum wavelength is 1.5 μm. The dotted lines in Fig. 8 indicate the effective indices of the two lowest TE modes (labeled mode A and mode B) of the GADC structure. By conventional coupled mode theory, a complete exchange of optical energy between the two slabs occurs if the difference between the effective indices of the modes that

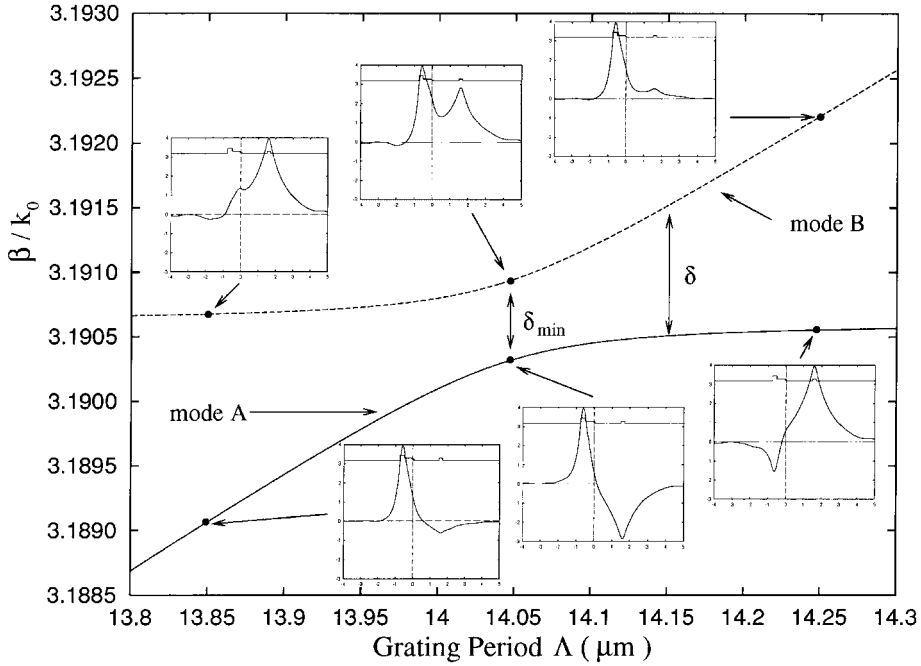

(a)

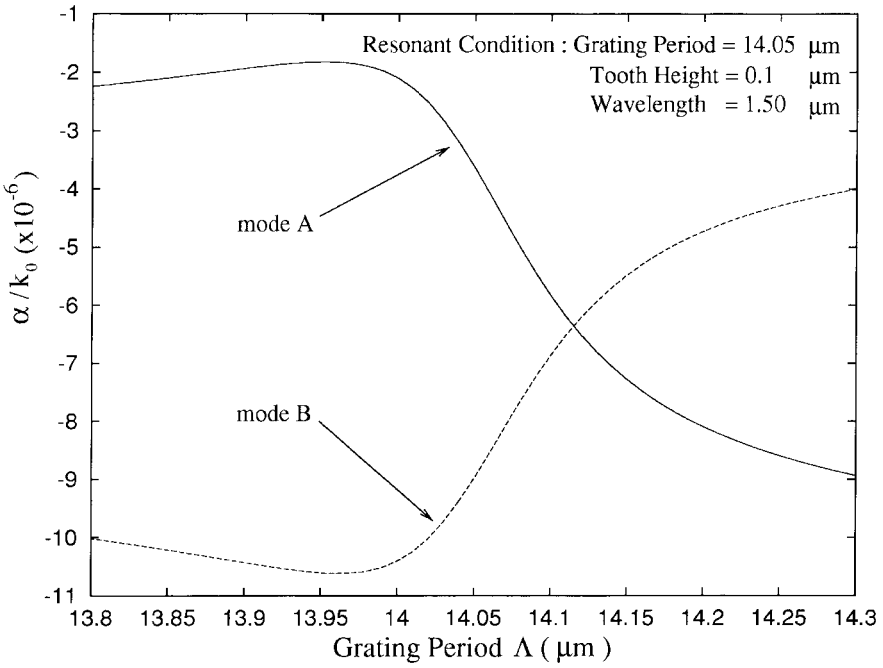

(b)

Fig. 9. The normalized (a) real part and (b) imaginary part of the propagation constants for modes A and B as a function of the grating period. The insets in (a) show the field distributions of mode A and mode B at and near resonance.

are to be coupled satisfies the relationship [3]

$$|n_A - n_B| = \frac{K}{k_0} = \frac{\lambda_0}{\Lambda} \tag{37}$$

where Λ is the length of one period of the grating, λ_0 is the wavelength, and n_A and n_B are the effective indices of modes A and B when the grating is absent. Since n_A and n_B are calculated without a grating, (37) is an approximate formula for the grating period.

We can obtain exact values for n_A and n_B by including the grating layer and using the Floquet–Block theory. Dispersion curves of the two modes of the GADC structure are found as a function of the grating period. Fig. 9 shows the normalized propagation constants of modes A and B as a function of the grating period where Fig. 9(a) and (b) correspond to the real and the imaginary parts of the propagation constants, respectively. In the vicinity of resonance, the two curves in Fig. 9(a) do not intersect. According to the analysis of the nongrating

directional coupler [4], the magnitudes of the two modes are nearly identical at resonance. Similarly, the resonant condition of a GADC structure can be determined by examining the total field distributions of the two modes. The field distributions of mode A and mode B [Fig. 9(a)] have large intensities in both subwaveguides when the difference between the real parts of the longitudinal propagation constants $(\delta = \beta_A - \beta_B - K)$ is minimized, in which case the coupling between the two subwaveguides is maximum. For this GADC structure excited with radiation with a free space wavelength of 1.5 μm, the resonant condition corresponds to a grating period of 14.05 μm.

Because of the grating, the modes of the GADC structure are expanded in an infinite number of space harmonics. Fig. 10(a) and (b) show the spatial harmonics for mode A and mode B at the resonant condition where the grating period is 14.05 μm. The duty cycle is 50% for the GADC structure in this paper. There are two space harmonics for these modes which have significant amplitudes. For mode A, the $n = 0$ and -1 harmonics are dominant while the other space harmonics are negligible. For mode B, the $n = 0$ and 1 harmonics are dominant, while the other harmonics are negligible. Note that the $n = 0$ harmonic of mode A and the $n = 1$ harmonic of mode B have similar field distributions which are both similar to the zero order mode of the structure without a grating in Fig. 6(a). Similarly, the $n = -1$ harmonic of mode A and the $n = 0$ harmonic of mode B also have similar field distributions which are both similar to the first order mode of the structure without a grating in Fig. 6(b). The complete field pattern is obtained by the summation of all space harmonics. Fig. 11(a) and (b) show the total field distributions of modes A and B. We obtain the "in-phase" (no zero-crossings of the electric field distribution between the subwaveguides) solution for mode B and the "out-of-phase" (a single zero-crossing of the electric field distribution between the subwaveguides) solution for mode A. Moreover, in subwaveguide B, the field of mode A has almost the same amplitude but a different sign as the field of mode B, while both modes have the same amplitudes in subwaveguide A. This means that these two modes can be superimposed so that their fields nearly cancel in subwaveguide B with most of the intensity in subwaveguide A at the input end of the coupler. Since both modes have negligible amplitude attenuations α_A and α_B [see Fig. 9(b)], their relative phases will reverse at a distance which is called the coupling length L_c. At this point the sum of the two modes superimpose so that most of the intensity is now in subwaveguide B.

Fig. 12(a) shows that the two modes are superimposed to yield an initial excitation in subwaveguide A. At the coupling length $z = 1.168$ mm, the power has been coupled over to subwaveguide B as shown in Fig. 12(b). This result is in good agreement (<10%) with that reported in [14]. Because both field distributions of modes A and B have some nonzero amplitude in the other subwaveguide, complete power exchange cannot be achieved. After traversing the coupling length distance, a small amount of residual energy will still exist in the input subwaveguide.

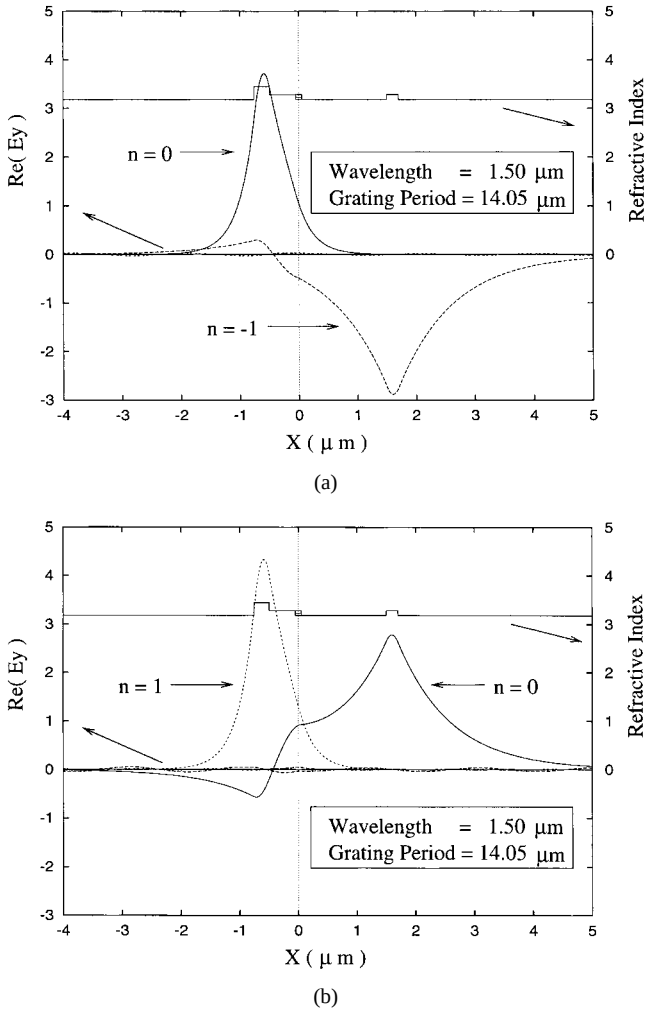

Fig. 10. The real part of the amplitudes of the space harmonics for (a) mode A and (b) mode B.

The powers in subwaveguides A and B are estimated by [35]

$$P_A = -\tfrac{1}{2}\,\mathrm{Re}\left\{\int_{-\infty}^{0} E_y H_x^*\,dx\right\}$$

and

$$P_B = -\tfrac{1}{2}\,\mathrm{Re}\left\{\int_{0}^{\infty} E_y H_x^*\,dx\right\}$$

for the TE mode. Fig. 13(a) shows the output powers through subwaveguides A and B as a function of the propagation distance z at the resonant condition $(\Lambda = 14.05\,\mu\mathrm{m}, \lambda = 1.50\,\mu\mathrm{m})$. At the input, most of the power is excited in subwaveguide A, and at a distance of 1.168 mm, a maximum of 92% of the power has transferred to subwaveguide B. The fine oscillations in Fig. 13 have a period equal to that of the grating [18]. If the grating period is not at the resonant condition, both the power coupling and the coupling length will decrease. Fig. 13(b) shows the ratios of the power in subwaveguides A and B versus the propagation distance z for a grating period of 14 μm. In this case, a maximum of 78% of the total power transfers from subwaveguide A to subwaveguide B in a distance of 0.749 mm. When the grating

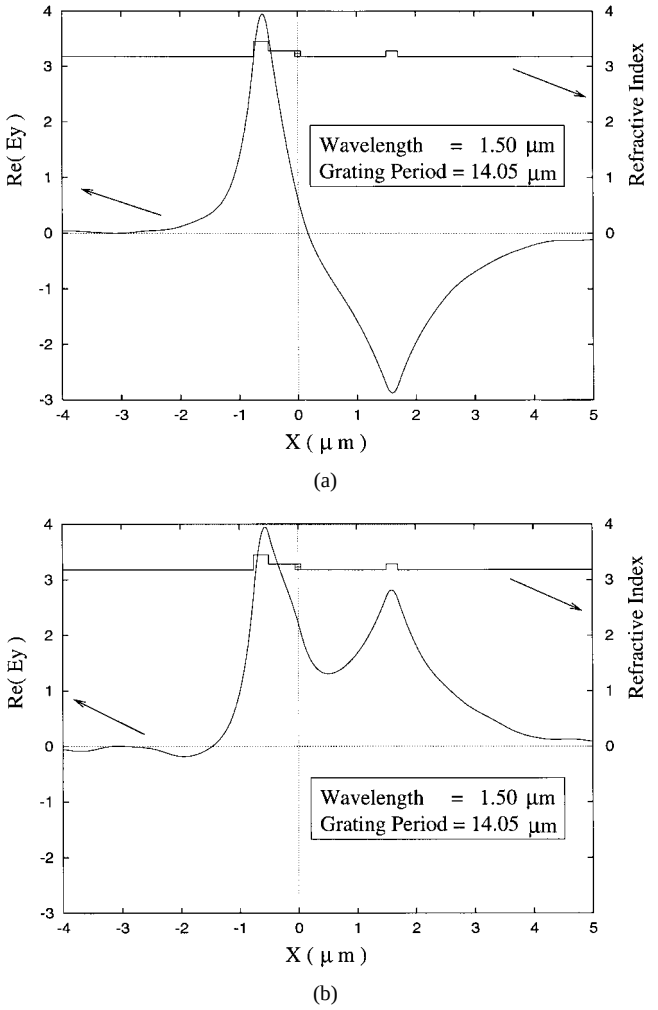

Fig. 11. The real part of the total field distributions for (a) mode A and (b) mode B.

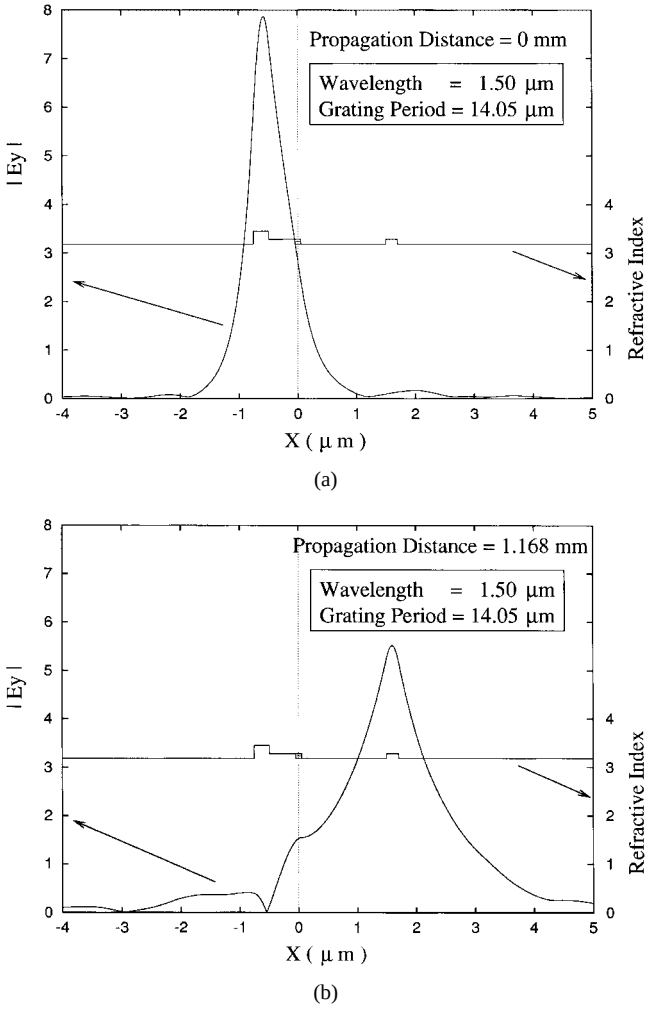

Fig. 12. The magnitude of the sum of the field distributions of modes A and B. The propagation distances are (a) $z = 0$ mm and (b) $z = 1.168$ mm.

period is reduced by 0.35%, the coupling length decreases by 36% and the coupled power is reduced by 14%.

Fig. 14 shows the dispersion and attenuation diagrams of the GADC structure as described in Table II. The minimum difference of β_A and β_B occurs at the wavelength of 1.5 μm (for a grating period of 14.05 μm) while the attenuations of the two modes are different but negligible. Fig. 15 shows the guided power in subwaveguides A and B as a function of the propagation distance away from resonance ($\lambda = 1.505\,\mu$m). The 0.3% change in wavelength reduces the coupling length by 22% and the coupling power by 38%.

VI. The Coupling Length Formula

This analysis of GADC structures is similar to that of nongrating couplers [4] in that (1) at resonance, the field distribution of the in-phase and out-of-phase modes both have significant power in each subwaveguides and (2) the input (or any) field distribution of the coupler is a superposition of the in-phase and out-of-phase modes of the structure. Just as an expression for the coupling length of conventional (nongrating) couplers can be simply derived from the two properties above, we can derive a similar formula for the coupling length of a GADC structure:

From Fig. 10, only two space harmonics of modes A or B are dominant at the resonant condition, while the others are negligible. While the total field is expressed as

$$\Psi(x,z) = e^{-j(\beta+j\alpha)z} \sum_{n=-\infty}^{\infty} f_n(x) e^{-jnKz}$$

the field distributions of modes A and B can be approximated as

$$\Psi^A(x,z) \approx e^{-j\beta_A z}[f_0^A(x) + f_{-1}^A(x) \cdot e^{jKz}]e^{\alpha_A z} \tag{38}$$

and

$$\Psi^B(x,z) \approx e^{-j\beta_B z}[f_0^B(x) + f_1^B(x) \cdot e^{jKz}]e^{\alpha_B z} \tag{39}$$

where

$$f_n(x) = \begin{cases} f_n^{(1)}(x), & x \in \text{layer } 1 \\ \vdots & \\ f_n^{(i)}(x), & x \in \text{layer } i \\ \vdots & \\ f_n^{(s)}(x), & x \in \text{layer } s. \end{cases}$$

Since the $n = 0$ harmonic of mode A is similar to the $n = 1$ harmonic of mode B, and the $n = -1$ harmonic of mode A

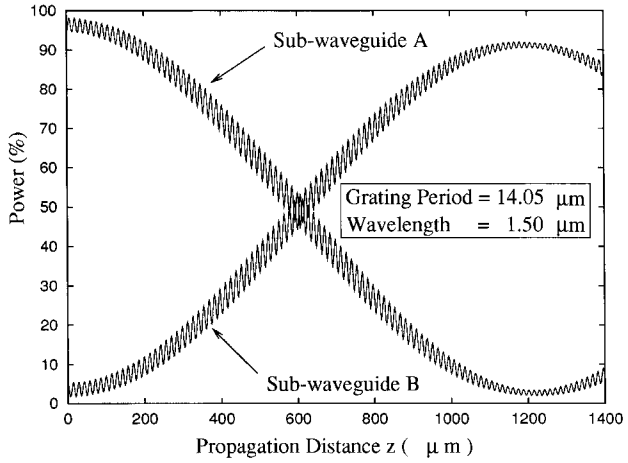

(a)

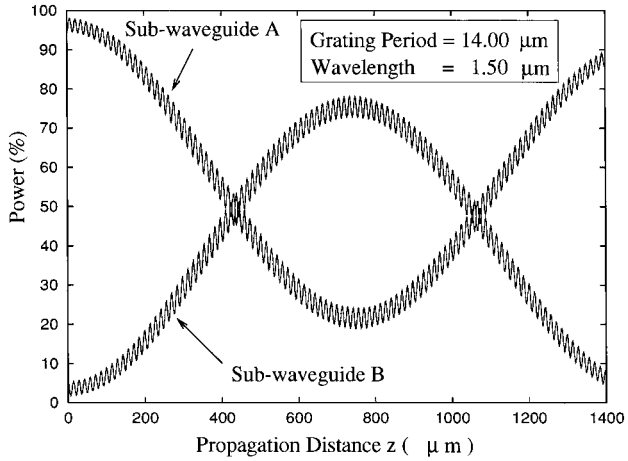

(b)

Fig. 13. The approximate power distributions in subwaveguides A and B as a function of the propagation distance with a grating period of (a) 14.05 μm and (b) 14.00 μm and a wavelength of 1.5 μm.

is similar to the $n = 0$ harmonic of mode B, we can make the approximation

$$f_0^A(x) \approx f_1^B(x) \tag{40a}$$

$$f_{-1}^A(x) \approx -f_0^B(x). \tag{40b}$$

From $\beta_B = \beta_A - K - \delta$, we have

$$e^{-j\beta_B z} = e^{-j\beta_A z} e^{-jKz} e^{-j\delta z}. \tag{41}$$

After substituting (41) into (39) and assuming

$$\alpha_A \approx \alpha_B \tag{42}$$

we find

$$\begin{aligned}\Psi^B(x,z) &\approx e^{-j\beta_A z}[f_0^B(x)e^{jKz} + f_1^B(x)]e^{\alpha_A z}e^{-j\delta z} \\ &= e^{-j\beta_A z}[f_0^A(x) - f_{-1}^A(x)e^{jKz}]e^{\alpha_A z}e^{-j\delta z}.\end{aligned} \tag{43}$$

Superimposing Ψ^A and Ψ^B at the input end $(z = 0)$, the amplitude of the sum is written as

$$|\Psi^A + \Psi^B| \approx 2|f_0^A|, \tag{44}$$

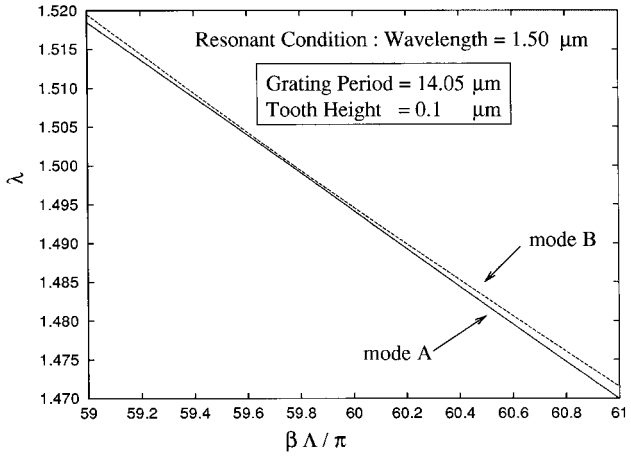

(a)

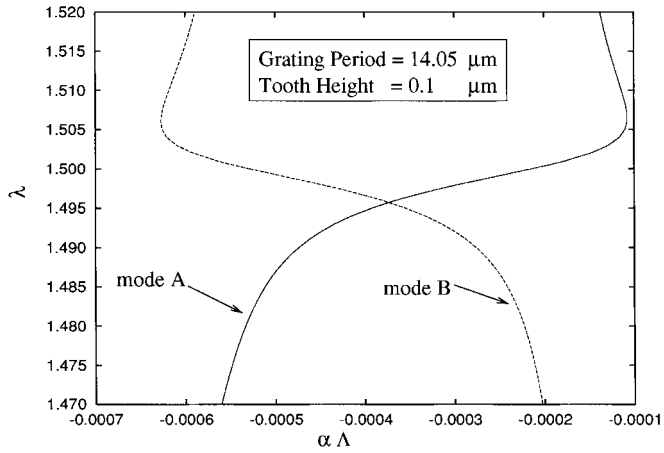

(b)

Fig. 14. (a) Dispersion and (b) attenuation diagrams for modes A and B.

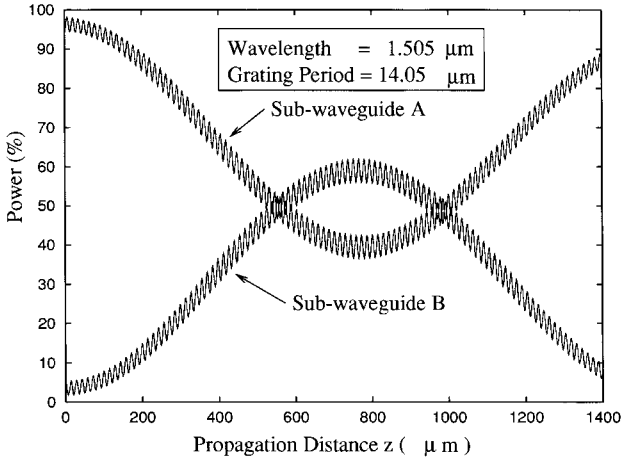

Fig. 15. Approximate power distributions in subwaveguides A and B as a function of the propagation distance with a grating period of 14.05 μm and a wavelength of 1.505 μm.

When the propagation distance z is equal to

$$L_c = \frac{\pi}{\delta} \tag{45}$$

Ψ^B reverses its phase, and the amplitude of the superposition of Ψ^A and Ψ^B becomes

$$|\Psi^A + \Psi^B| \approx 2|f_{-1}^A|. \tag{46}$$

f_0^A has a field distribution that is predominately concentrated in subwaveguide A, while f_{-1}^A has a field distribution that is predominately confined to subwaveguide B. Accordingly, maximum power is shifted from subwaveguide A to subwaveguide B in a length L_c.

When the two modes have almost equal attenuation [see (42)], (45) can estimate the coupling length without computing the power distribution along the propagation distance. For the GADC structure shown in Table II, the estimated coupling length from (45) is 1.208 mm. Compared with the result plotted in Fig. 13(a), the relative error is about 3.3%.

VII. The Truncation Accuracy

In practice, the infinite number of space harmonics must be truncated. Since the leaky space harmonics in the periodic dielectric waveguide determine the attenuation of the mode, it is important to consider them and develop a procedure for determining the significant harmonics.

By varying the positive and negative space harmonics, we can examine the accuracy of the propagation constants. For the real part of the propagation constants, the relative errors are less than 10^{-7} if seven space harmonics ($n = -3$ to 3) are used. The imaginary parts of the propagation constants are sensitive to the negative harmonics because these negative harmonics represent leaky waves which produce radiation loss.

From the dispersion curve in Fig. 14(a), almost 59 negative harmonics are leaky. However, we find that using the $n = -8$ to 3 space harmonics results in a computational error of less than 6% for the attenuation. Therefore, 12 space harmonics were used in all the numerical calculations for this paper.

VIII. Conclusion

In this paper we used a complete Floquet–Bloch solution to analyze grating-assisted directional couplers. We show that the presence of the grating greatly alters the modes of the composite structure near resonance so that the "in-phase" and "out-of-phase" modes have similar amplitudes in both subwaveguide regions. As a result, the grating-assisted coupling process is conceptually similar to that found in conventional (nongrating) couplers. If the attenuation of both modes is similar, a simple formula describes the coupling length.

We also present a modification of the conventional rule for choosing branch cuts that gives a physically consistent choice for proper and improper space harmonics, yet maintains the continuity of the propagation constant as k_0 is continuously varied.

The analysis developed in this paper agrees with the results of previously published grating-assisted directional couplers analyzed by coupled mode theory. However, this more general approach can be applied to composite waveguides where one of the modes is leaky, and/or where the two modes have significantly different attenuation.

Appendix

A system of first-order differential equations representing Maxwell's equations is written in vector form

$$\frac{d}{dx}\begin{pmatrix}\overline{f}(x)\\ \overline{g}(x)\end{pmatrix} = \boldsymbol{A}(k_{z0})\begin{pmatrix}\overline{f}(x)\\ \overline{g}(x)\end{pmatrix} \tag{A1}$$

where the square matrix $\boldsymbol{A}(k_{z0})$

$$\boldsymbol{A}(k_{z0}) = \begin{pmatrix}0 & \boldsymbol{Q}(k_{z0})\\ \boldsymbol{P}(k_{z0}) & 0\end{pmatrix} \tag{A2}$$

is formed from the two matrices $\boldsymbol{P}(k_{z0})$ and $\boldsymbol{Q}(k_{z0})$ [see (21) and (22)]. If we assume that layer k is the grating layer, the interfaces of the grating layer are at $x = x_{k-1}$ and $x = x_k$. We define the vector $\overline{y}(x)$ [see (20)] as

$$\overline{y}(x) = \begin{pmatrix}\overline{f}(x)\\ \overline{g}(x)\end{pmatrix}. \tag{A3}$$

By applying the boundary condition [see (28)] at $x = x_{k-1}, \overline{g}(x_{k-1})$ can be found from $\overline{f}(x_{k-1})$ so that $\overline{y}(x_{k-1})$ can be expressed as

$$\overline{y}(x_{k-1}) = \begin{pmatrix}\overline{f}(x_{k-1})\\ \overline{g}(x_{k-1})\end{pmatrix} = \boldsymbol{Y}_0 \cdot \begin{pmatrix}\overline{f}(x_{k-1})\\ \overline{f}(x_{k-1})\end{pmatrix} \tag{A4}$$

where

$$\boldsymbol{Y}_0(k_{z0}) = \begin{pmatrix}\boldsymbol{I} & 0\\ 0 & \boldsymbol{G}(k_{z0})\end{pmatrix} \tag{A5}$$

and $\boldsymbol{G}(k_{z0}) = \boldsymbol{Q}^{-1}(k_{z0}) \cdot \boldsymbol{U}^{-1}(x_{k-1}) \cdot \boldsymbol{V}(x_{k-1})$. Substituting (A3) into (A1), we obtain

$$\frac{d\overline{y}(x)}{dx} = \boldsymbol{A}(k_{z0}) \cdot \overline{y}(x). \tag{A6}$$

By using the Runge–Kutta method, the grating region is divided into v intervals with a step size of $h = t_k/v$ where t_k is the thickness of the grating layer. The classical fourth-order Runge–Kutta method produces

$$\overline{k}_1 = h \cdot \boldsymbol{A}(k_{z0}) \cdot \overline{y}_j = \boldsymbol{K}_1 \overline{y}_j \tag{A7}$$

$$\overline{k}_2 = h \cdot \boldsymbol{A}(k_{z0}) \cdot (\overline{y}_j + \tfrac{1}{2}\overline{k}_1) = \boldsymbol{K}_2 \overline{y}_j \tag{A8}$$

$$\overline{k}_3 = h \cdot \boldsymbol{A}(k_{z0}) \cdot (\overline{y}_j + \tfrac{1}{2}\overline{k}_2) = \boldsymbol{K}_3 \overline{y}_j \tag{A9}$$

$$\overline{k}_4 = h \cdot \boldsymbol{A}(k_{z0}) \cdot (\overline{y}_j + \overline{k}_3) = \boldsymbol{K}_4 \overline{y}_j \tag{A10}$$

and

$$\overline{y}_{j+1} = \overline{y}_j + \tfrac{1}{6}\left(\overline{k}_1 + 2\overline{k}_2 + 2\overline{k}_3 + \overline{k}_4\right) \tag{A11}$$

for each $j = 1, \cdots, v$. Since the initial value of $\overline{y}$ is set at $x = x_{k-1}$ and is written as

$$\overline{y}_1 = \overline{y}(x_{k-1}) = \begin{pmatrix}\overline{f}(x_{k-1})\\ \overline{g}(x_{k-1})\end{pmatrix} \tag{A12}$$

$\overline{y}(x_k)$ can be expressed as

$$\overline{y}(x_k) = \overline{y}_v = \boldsymbol{Y}_v(k_{z0}) \cdot \overline{y}_1 = \boldsymbol{Y}_v(k_{z0}) \cdot \overline{y}(x_{k-1}). \quad \text{(A13)}$$

Substituting (A4) into (A13), we obtain

$$\begin{aligned}\overline{y}(x_k) &= \begin{pmatrix}\overline{f}(x_k)\\ \overline{g}(x_k)\end{pmatrix} = \boldsymbol{Y}_v(k_{z0}) \cdot \overline{y}(x_{k-1}) \\ &= \boldsymbol{Y}_v(k_{z0}) \cdot \boldsymbol{Y}_0(k_{z0}) \cdot \begin{pmatrix}\overline{f}(x_{k-1})\\ \overline{f}(x_{k-1})\end{pmatrix} \\ &= \boldsymbol{Y}(k_{z0}) \cdot \begin{pmatrix}\overline{f}(x_{k-1})\\ \overline{f}(x_{k-1})\end{pmatrix}. \end{aligned} \quad \text{(A14)}$$

Since $\overline{f}(x_k)$ and $\overline{g}(x_k)$ are given by

$$\begin{aligned}\begin{pmatrix}\overline{f}(x_k)\\ \overline{g}(x_k)\end{pmatrix} &= \boldsymbol{Y}(k_{z0}) \begin{pmatrix}\overline{f}(x_{k-1})\\ \overline{f}(x_{k-1})\end{pmatrix} \\ &= \begin{pmatrix}\boldsymbol{Y}_{11}(k_{z0}) & \boldsymbol{Y}_{12}(k_{z0})\\ \boldsymbol{Y}_{21}(k_{z0}) & \boldsymbol{Y}_{22}(k_{z0})\end{pmatrix} \begin{pmatrix}\overline{f}(x_{k-1})\\ \overline{f}(x_{k-1})\end{pmatrix} \end{aligned} \quad \text{(A15)}$$

$\overline{f}(x_k)$ and $\overline{g}(x_k)$ can be rewritten as

$$\begin{aligned}\overline{f}(x_k) &= (\boldsymbol{Y}_{11}(k_{z0}) + \boldsymbol{Y}_{12}(k_{z0})) \cdot \overline{f}(x_{k-1}) \\ &= \boldsymbol{Y}_f(k_{z0}) \cdot \overline{f}(x_{k-1}) \quad \text{(A16a)} \\ \overline{g}(x_k) &= (\boldsymbol{Y}_{21}(k_{z0}) + \boldsymbol{Y}_{22}(k_{z0})) \cdot \overline{f}(x_{k-1}) \\ &= \boldsymbol{Y}_g(k_{z0}) \cdot \overline{f}(x_{k-1}) \quad \text{(A16b)}\end{aligned}$$

where $\boldsymbol{Y}_f(k_{z0})$ and $\boldsymbol{Y}_g(k_{z0})$ are given by

$$\begin{aligned}\boldsymbol{Y}_f(k_{z0}) &= \boldsymbol{Y}_{11}(k_{z0}) + \boldsymbol{Y}_{11}(k_{z0}) \quad \text{(A17a)} \\ \boldsymbol{Y}_g(k_{z0}) &= \boldsymbol{Y}_{21}(k_{z0}) + \boldsymbol{Y}_{22}(k_{z0}). \quad \text{(A17b)}\end{aligned}$$

REFERENCES

[1] A. Hardy and W. Streifer, "Coupled mode theory of parallel waveguides," *J. Lightwave Technol.*, vol. LT-3, pp. 1135–1146, Oct. 1985.

[2] E. Marcatili, "Improved coupled-mode equations for dielectric guides," *IEEE J. Quantum Electron.*, vol. QE-22, pp. 988–993, 1986.

[3] R. G. Hunsperger, *Integrated Optics: Theory and Technology*, 2nd ed. Berlin, Germany: Springer-Verlag, 1984.

[4] D. Marcuse, "Directional couplers made of nonidentical asymmetric slabs. Part I: Synchronous couplers," *J. Lightwave Technol.*, vol. LT-5, pp. 113–118, Jan. 1987.

[5] T. L. Koch, E. G. Burkhardt, F. G. Storz, T. J. Bridges, and T. Sizer, II, "Vertically grating-coupled ARROW structures for III-V integrated optics," *IEEE J. Quantum Electron.*, vol. QE-23, pp. 889–897, June 1987.

[6] T. L. Koch, P. J. Corvini, W. T. Tsang, U. Koren, and B. I. Miller, "Wavelength selective interlayer directionally grating-coupled InP/InGaAsP waveguide photodetection," *Appl. Phys. Lett.*, vol. 51, no. 14, pp. 1060–1062, 1987.

[7] L. L. Buhl, R. C. Alferness, U. Koren, B. I. Miller, M. G. Young, T. L. Koch, C. A. Burrus and G. Raybon, "Grating assisted vertical coupler/filter for extended tuning range," *Electron. Lett.*, vol. 29, no. 1, pp. 81–82, Jan. 1993.

[8] H. Sakata and S. Takeuchi, "Grating-assisted coupler filters using AlGaAs/GaAs MQW waveguides," *IEEE Photon. Technol. Lett.*, vol. 3, pp. 899–901, Oct. 1991.

[9] R. C. Alferness, L. L. Buhl, U. Koren, B. I. Miller, M. G. Young, T. L. Koch, C. A. Burrus and G. Raybon, "Broadly tunable InGaAsP/InP buried rib waveguide vertical coupler filter," *Appl. Phys. Lett.*, vol. 60, no. 8, pp. 980–982, 1992.

[10] C. Cremer, G. Heise, R. Marz, H. Riechert, and M. Schienle, "InGaAsP Y-branch grating demultiplexer," *Electron. Lett.*, vol. 23, no. 7, pp. 321–322, 1987.

[11] J. M. Senior and S. D. Cusworth, "Devices for wavelength multiplexing and demultiplexing," *Inst. Elec. Eng. Proc.*, vol. 136, Pt. J, no. 3, pp. 183–202, 1989.

[12] G. R. Hill, "Wavelength domain optical network techniques," in *Proc. IEEE*, vol. 77, pp. 121–132, 1989.

[13] D. Marcuse, "Directional couplers made of nonidentical asymmetrical slabs. Part II: Grating- assisted couplers," *J. Lightwave Technol.*, vol. LT-5, pp. 268–273, Feb. 1987.

[14] ——, "Radiation loss of grating-assisted directional coupler," *IEEE J. Quantum Electron.*, vol. QE-26, pp. 675–684, Apr. 1990.

[15] ——, *Theory of Dielectric Optical Waveguides*, 2nd ed. New York: Academic, 1991.

[16] W. P. Huang and H. A. Haus, "Power exchange in grating-assisted couplers," *J. Lightwave Technol.*, vol. 7, pp. 920–924, June 1989.

[17] H. A. Haus, W. P. Huang, S. Kawakami, and N. A. Whitaker, "Coupled-mode theory of optical waveguides," *J. Lightwave Technol.*, vol. LT-5, pp. 16–23, 1987.

[18] W. P. Huang, B. E. Little, and S. K. Chaudhuri, "A new approach to grating-assisted couplers," *J. Lightwave Technol.*, vol. 9, pp. 721–727, June 1991.

[19] W. P. Huang and J. W. Y. Lit, "Nonorthogonal coupled-mode theory of grating-assisted codirectional couplers," *J. Lightwave Technol.*, vol. 9, pp. 845–852, July 1991.

[20] W. P. Huang and J. Hong, "A transfer matrix approach based on local normal modes for coupled waveguides with periodic perturbations," *J. Lightwave Technol.*, vol. 10, pp. 1367–1375, Oct. 1992.

[21] W. P. Huang, J. Hong, and Z. M. Mao, "Improved coupled-mode formulation based on composite modes for parallel grating-assisted co-directional couplers," *IEEE J. Quantum Electron.*, vol. QE-29, pp. 2805–2812, Nov. 1993.

[22] B. E. Little, W. P. Huang, and S. K. Chaudhuri, "A multiple-scale analysis of grating-assisted couplers," *J. Lightwave Technol.*, vol. 9, pp. 1254–1263, Oct. 1991.

[23] B. E. Little and H. A. Haus, "A variational coupled-mode theory for periodic waveguides," *IEEE J. Quantum Electron.*, vol. QE-31, pp. 2258–2264, 1995.

[24] B. E. Little, "A variational coupled-mode theory including radiation loss for grating-assisted couplers," *J. Lightwave Technol.*, vol. 14, pp. 188–195, Feb. 1996.

[25] V. M. N. Passaro and M. N. Aremise, "Analysis of radiation loss in grating-assisted codirectional couplers," *IEEE J. Quantum Electron.*, to be published.

[26] S. T. Peng, T. Tamir, and H. L. Bertoni, "Theory of periodic dielectric waveguides," *IEEE Trans. Microwave Theory Tech.*, vol. MTT-23, pp. 123–133, Jan. 1975.

[27] W. Streifer, D. R. Scifres, and R. D. Burnham, "Analysis of grating-coupled radiation in GaAs:GaAlAs lasers and waveguides," *IEEE J. Quantum Electron.*, vol. 12, pp. 422–428, July 1976.

[28] K. C. Chang, V. Shah, and T. Tamir, "Scattering and guiding of waves by dielectric gratings with arbitrary profiles," *J. Opt. Soc. Amer.*, vol. 70, no. 7, pp. 804–813, July 1980.

[29] G. Hadjicostas, J. K. Butler, G. A. Evans, N. W. Carlson, and R. Amantea, "A numerical investigation of wave interactions in dielectric waveguides with periodic surface corrugations," *IEEE J. Quantum Electron.*, vol. 26, pp. 893–902, May 1990.

[30] J. K. Butler, W. E. Ferguson, Jr., Gary A. Evans, and P. J. Stabile, "A boundary element technique applied to the analysis of waveguides with periodic surface corrugations," *IEEE J. Quantum Electron.*, vol. 28, pp. 1701–1709, July 1992.

[31] R. E. Collin and F. J. Zucker, Eds., *Antenna Theory*, vol. 2. New York: McGraw-Hill, 1969, sec. 19.10, p. 203.

[32] R. L. Burden and J. D. Faires, *Numerical Analysis*, 4th ed. Boston, MA: PWS-KENT, 1984.

[33] J. Jacobsen, "Analytical, numerical, and experimental investigation of guided waves on a periodically strip-loaded dielectric slab," *IEEE Trans. Antennas Propagat.*, vol. AP-18, pp. 370–387, May 1970.

[34] M. Matsumoto, M. Tsutsumi, and N. Kumagai, "Bragg reflection characteristics of millimeter waves in a periodically plasma-induced semiconductor waveguide," *IEEE Trans. Microwave Theory Tech.*, vol. MTT-34, pp. 406–411, Apr. 1986.

[35] W. P. Huang, "Coupled-mode theory for optical waveguides: an overview," *J. Opt. Soc. Amer. A*, vol. 11, no. 3 ,pp. 963–983, Mar. 1994.

Nai-Hsiang Sun (S'93–M'97) was born in Tainan, Taiwan, R.O.C., in 1962. He received the B.S. degree in electronic engineering from Chung Yuan Christian University, Chungli, Taiwan, in 1984, the M.S. degree in electrical engineering from the National Cheng Kung University, Tainan, Taiwan, in 1986, and the Ph.D. degree in electrical engineering from Southern Methodist University, Dallas, TX, in 1997.

In 1997, he joined the faculty of Electrical Engineering at the I-Shou University, Kauhsiung, Taiwan, where he is an Assistant Professor. His current research interest is in the area of photonic integrated wavelength division multiplexing sources, periodic dielectric waveguides, and numerical modeling of semiconductor lasers.

Jerome K. Butler was born in Shreveport, LA. He received the B.S.E.E. degree from Louisiana Polytechnic Institute, Ruston, and the M.S.E.E. and Ph.D.degrees from the University of Kansas, Lawrence.

He was a Research Assistant and held a CRES Fellowship at the Center for Research in Engineering Sciences, University of Kansas. He conducted research concerned with electromagnetic wave propagation and the optimization and synthesis techniques of antenna arrays. He joined the faculty of the School of Engineering and Applied Science, Southern Methodist University, Dallas, TX, where he is now a University Distinguished Professor of Electrical Engineering. His primary research areas are solid-state injection lasers, radiation and detection studies of lasers, millimeter-wave systems, integrated optics and the application of integrated optical circuits, and quantum electronics. In 1977, he was given the Southern Methodist University Sigma Xi Research Award. In the summers from 1969 to 1990, he was a Staff Scientist, at the David Sarnoff Research Center (formerly RCA Laboratories), Princeton, NJ. During the 1996–1997 academic year, he was on sabbatical leave with the Photonics and Micromachining System Components Laboratory at Texas Instruments. At present, he holds a consulting appointment with the Components and Materials Research Center at Texas Instruments, Dallas. He has also held consulting appointments with the Central Research Laboratory of Texas Instruments, Inc., the Geotechnical Corporation of Teledyne, Inc., Earl Cullum Associates of Dallas, Texas and the University of California Los Alamos Scientific Laboratory, Los Alamos, NM.

Dr. Butler is a member of Sigma Xi, Tau Beta Pi, and Eta Kappa Nu, and is a registered Professional Engineer in the State of Texas.

Gary A. Evans was born in Omak, WA. He received the B.S.E.E. degree from the University of Washington, Seattle, in 1970, and the M.S.E.E. and Ph.D. degrees in electrical engineering and physics from the California Institute of Technology, Pasadena, in 1971 and 1975, respectively.

After postdoctoral work at Caltech, he worked for R&D Associates, Marina Del Rey, CA, and was a Visiting Assistant Professor in the Electrical Engineering Department at the University of Washington (1977–1979). He has worked at the Aerospace Corporation, El Segundo, CA, (1979–1981), TRW, Redondo Beach, CA, (1981–1984), and RCA Laboratories (now Sarnoff Corporation), Princeton, NJ, (1984–1992). In 1992 he joined Southern Methodist University, Dallas, TX, as a Professor in the Electrical Engineering Department. Since 1979, he has primarily worked on the design, growth, and fabrication of conventional and surface emitting semiconductor lasers, has over 180 publications, and is a co-editor of the book *Surface Emitting Semiconductor Lasers* (New York: Academic).

Dr. Evans is a licensed professional engineer, has served on numerous IEEE committees, is a Past-Chairman of the Princeton Lasers and Electro-Optics Society (LEOS) Section, a past Chairman of the Santa Monica Bay Section of the IEEE, and from 1990 to 1996, was an Associate Editor of the IEEE JOURNAL OF QUANTUM ELECTRONICS.

Lily Pang received the B.S. degree in electrical engineering from University of California at Irvine in 1986. She also received the M.S. and Ph.D. degrees in electrical engineering from Massachusetts Institute of Technology, Cambridge, in1989 and 1993, respectively.

She jointed Central Research Laboratories of Texas Instruments, Dallas, in 1993, worked on silica-glass waveguide optical switches. Since 1995, she has been working on integrated silica-glass waveguide multiplexer coupled WDM semiconductor lasers, VCSEL's on Si-CMOS, and high-power efficient visible lasers.

Phil Congdon, photograph and biography not available at the time of publication.